Novel Neural Network-Based Load Frequency Control Scheme: A Case Study of Restructured Power System

**NAGENDRA KUMAR[1], HASMAT MALIK [ID][2], (Senior Member, IEEE),
AKHILESH SINGH[3], (Member, IEEE), MAJED A. ALOTAIBI [ID][4], (Member, IEEE),
AND MOHAMMED E. NASSAR[5], (Member, IEEE)**

[1]Department of Electrical & Electronics Engineering, G. L. Bajaj Institute of Technology & Management, Greater Noida, Uttar Pradesh 201306, India
[2]BEARS, University Town, NUS Campus, Singapore 138602
[3]Department of Electrical and Electronics Engineering, Seemant Institute of Technology Pithoragarh, Uttarakhand 262501, India
[4]Department of Electrical Engineering, College of Engineering, King Saud University, Riyadh 11421, Saudi Arabia
[5]Department of Electrical and Computer Engineering, University of Waterloo, Waterloo, ON N2L 3G1, Canada

Corresponding authors: Hasmat Malik (hasmat.malik@gmail.com) and Majed A. Alotaibi (majedalotaibi@ksu.edu.sa)

ABSTRACT Nowadays, neural networks (NN) are being utilized in different control problems because of their excellent ability to model any nonlinear process. NN is suitable for the process having a wide range of operating conditions. In this work, the neural network-based internal model control (NN-IMC) scheme has been considered as a secondary controller for the load frequency control (LFC) problem in the restructured electricity market in order to meet Poolco and bilateral transactions. The proposed control scheme has been implemented on a 75-bus, 15-generator power system. The test system is divided into four areas. It is seen that area frequency errors have been eliminated at a steady state in all cases, and Gencos/Discos shared the increase in demand as per their involvement in the frequency regulation market. The results show that the NN-IMC control scheme has good performance and improves system responses effectively. Further, the performance of the NN-IMC control scheme has also been compared with the fractional-order proportional-integral-derivative (FO-PID) control scheme It is observed that the performance of the FO-PID controller is superior to the NN-IMC scheme in terms of settling time and similar to the NN-IMC control scheme in terms of maximum overshoots/undershoots. The compliance of the NN-IMC scheme has also been checked with NERC standards. It is seen that the NN-IMC scheme also satisfied the CPS1 and CPS2 control standards.

INDEX TERMS BBBC, deregulation, FO-PID, LFC, NN-IMC, NERC, optimization.

NOMENCLATURE

Abbreviation/symbol	Description.
LFC	Load Frequency Control.
AGC	Automatic generation Control.
NN	Neural Network.
NN-IMC	Neural Network-Based Internal Model control.
FO/FO-PID	Fractional Order/ Fractional-Order Proportional-Integral-Derivative.
CPS/CF	Control Performance Standard/ Compliance factor.
BBBC/GA/PSO/ICA	Big Bang Big Crunch/Genetic alorithm/Particle sworm optimization/Imperialistic competition algorithm.
P_g/P_d	Generated/demanded power.
G/D	Genco/Disco.
DPM	Disco Participation Matrix.
NERC	North American Electric Reliability Corporation.
P/PI/PID	Proportional/ Proportional Integral/ Proportional Integral Derivative.
ACE	Area control error.
Ptie	Tie-line power.
f/R	Frequency/regulation(Hz/pu MW).
DIC	Direct inverse control.

I. INTRODUCTION

The power system is a large and complex engineering system with multiple control areas. Using tie-lines, each control area is connected to another. Therefore, keeping this system in balance is not an easy task. Any disruption or change in load demand may cause a change in system frequency, which can have major effects if not addressed quickly. For decades, load frequency control (LFC) has been claimed as one of the most vital power system services to keep system frequency and tie-line flow variations within limits [1]. The responsibility of LFC has been increased after deregulation of the power system, where the electricity sector is divided into separate entities like Gencos, Transcos, Discos, and others to balance generation and load demands. Although the core responsibility of LFC remains the same in a deregulated framework, the modifications associated with LFC in a deregulated environment have been addressed in [2]. The heart of LFC is the control scheme, which serves purposes like bringing back frequency to the nominal value, keeping interchange within limits to run the system at balance. In literature, control schemes based on classical, modern, robust, intelligent, etc., have been reported. Many researchers have also reported fuzzy, neural, and optimization algorithms, i.e. Ant colony, GA, PSO, ICA, etc., based control schemes [3], [4]. An adaptive load frequency control technique utilizing jay and ballon effect in isolated microgrid power system and two interconnected microgrids (MGs) has been presented in [5]. It is seen that I, PI and PID [6] are popular among researchers due to their merits, like simple construction, easy implementation, good performance, etc. The effectiveness of these control approaches has successfully been seen in many areas, from power systems to other systems. The Grasshopper optimization algorithm (GOA) based PID controllers are used for load frequency control of the hybrid microgrid system [7]. However, it has also been reported that this technique is not preferred when the number of parameters to be optimized is high. It is seen that for a step load change, the NN-based control scheme produces a better response than the conventional Proportional Integral (PI) controller [3], [8]. Internal model control (IMC) is one of the robust control methods and is easy to implement [9]–[11]. Therefore, in this work, IMC utilizing NN has been designed to take advantage of both NN and IMC. Nowadays, researchers focus on fractional-order (FO) control schemes as an alternative to classical control schemes [12]. These control schemes are being used in several engineering fields, including power systems [13], [14]. Disturbance Observer-based Fractional-order Integral Sliding Mode Frequency Control Strategy for Interconnected Power System has been implemented in [15]. Fractional-order controllers utilizing Gate Controlled Series Controllers (GCSC) to regulate the frequency in multi-area power systems considering time delays have been implemented in [16]. It is also evident that the performance of a control system is determined by its parameters. Therefore, to design a good control scheme, its parameters must be obtained optimally [17].

A Robust Control Scheme for Distributed Battery Energy Storage Systems in Load Frequency Control is reported in [18]. An MPC control scheme to regulate frequency in the presence of electric vehicles has been implemented on the isolated power system in [19]. The power system is being changed from a regulated to a deregulated environment because of the many advantages of a deregulated scenario. Therefore, the stability of the power system against uncertainties, noise, disturbance, etc., is a point of prime concern in this new environment. This increases the role and responsibility of the control approaches used in power systems [20]–[22]. The changing environment requires more efficient control schemes, which motivated authors to design a neural network-based internal model control (NN-IMC) scheme in order to investigate the LFC problem. The performance of the NN-IMC scheme has been compared with the FO-PID control scheme. The optimal parameters of the FO-PID control scheme have been determined by the Big Bang Big Crunch (BBBC) algorithm [23]. Indeed, there are many search algorithms such as particle swarm optimization (PSO), differential evaluation (DE), genetic algorithm (GA) etc., available in the literature. Authors had already compared three optimization algorithms for the problem of AGC, and applied BBBC for finding the optimal parameters of FO-PID controller on the basis of its comparison with other search algorithms, namely ICA and GA [24]–[27]. In the comparison, it had been found that BBBC algorithm gives better results than other two search algorithms. The best convergence (minimum cost versus iteration) results show that BBBC convergence speed is better than ICA and GA to provide optimal gains of the controller for the same design parameter. A 75-bus, 15 generator system, divided into four control areas, has been considered as a test system. The traditional power system is undergoing numerous reforms as a result of deregulation. A Disco can now have power contracts with Gencos in its area or from another area, and this type of power transaction is referred to as bilateral trading, which is implemented using the Disco Participation Matrix (DPM) [28]. The other mode of power contract is known as the Poolco transaction. Therefore, a variety of load disturbances along with both (Poolco + bilateral) power transactions have been simulated to check the performance of the designed control schemes, which are calculated in terms of settling time, oscillations in various time-domain responses. A comparison shows that both control approaches are settling the targeted parameters at their desired values at steady state. The compliance with NERC has also been checked with both the control schemes. The distinct features of this paper are as follows:

- An NN-IMC control scheme is considered for frequency control of the 75-bus, 15 generators (four-area) deregulated hydro-thermal power system.
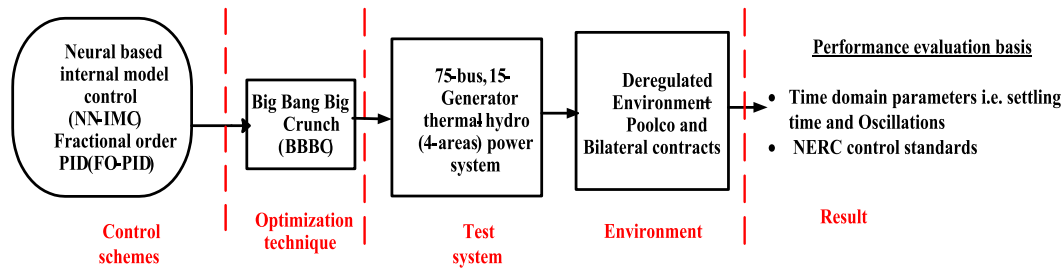- Poolco and bilateral power transactions between Gencos and Discos in different areas.
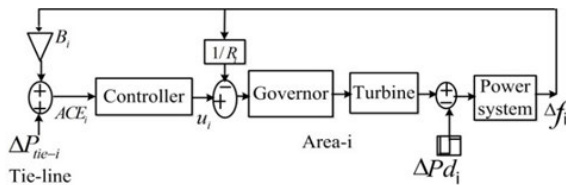
FIGURE 1. Graphical abstract.

FIGURE 2. Block diagram of a single control area, i.

- Power transaction violation case has also been considered to check the robustness of the designed control schemes.
- Compliance with NERC control standards has been checked.
- A comparative study between NN-IMC and FO-PID is carried out.

Figure 1 depicts a graphical abstract of the research presented in this article. Control schemes, optimization techniques, test systems, environments, and findings are all shown in the graphical abstract. The rest of this article is organized as follows: The modelling of multiarea power systems is introduced in section 2. Section 3 explains the considered control schemes. The simulation results and discussions are presented in Section 4. Section 5 deals with NERC control standards. Finally, in section 6, the complete analysis has been concluded.

II. MODELLING OF MULTIAREA POWER SYSTEM IN DEREGULATED ENVIRONMENT

The power system is an interconnection of several control areas, which consist of their own generation, transmission and distribution. Therefore, to model the LFC scheme for a multiarea system, a single control area is considered((e.g. *i*). This control area consists of the governor, turbine, generator, load, and a control scheme to keep the system at balance by keeping frequency and interarea power at their scheduled values. The block diagram representation of ith control area is shown in Figure 2, where Δf_i is the deviation in system frequency (Hz).

ΔP_{tie-i} Shows a deviation in tie-line flow (pu MW). ΔP_d shows incremental change in load (pu MW). R_i denotes

governor regulation (Hz/pu MW). B_i is frequency bias (pu MW/Hz). u_i is the control signal of ith area.

Any deviation in load demand results in the formation of an area control error (ACE_i), which is the weighted sum of tie-line and frequency deviations (1).

$$ACE_i = B_i \Delta F_i + \Delta Ptie_i \tag{1}$$

In conventional power systems, the main role of the control scheme is to eliminate this ACE only. In a deregulated environment, different transactions like Poolco, bilateral, and combinations of both are being used for power transactions under the supervision of ISO for successful operation of the power system. These bilateral transactions have an effect on tie-line power, such that the scheduled tie-line flow can change as given in (2) [24]–[27].

$$\Delta Ptie_{i\text{-new}} = \Delta Ptie_i + \sum_{\substack{k=1 \\ i \neq k}}^{n} D_{ik} - \sum_{\substack{k=1 \\ i \neq k}}^{n} D_{ki} \tag{2}$$

where n = total areas, D_{ik} = Disco demand (k[th] area) to the Genco (i[th] area), D_{ki} = Disco demand (i[th] area) to the Genco (k[th] area). ΔP_{tie-i} is tie-line variation without bilateral transaction. Eq. (2) further modifies the existing ACE as given in (3).

$$ACE_i = B_i \Delta F_i + \Delta Ptie_{i\text{-new}} \tag{3}$$

The LFC scheme regulates the output of generators to meet deviations in load demand to nullify the ACE given in (3). This change in generation for bilateral transactions can be determined using (4)

$$\Delta P_{gi} = \sum_j cpf_{ij} \Delta P_{Dj} \tag{4}$$

These changes and modifications in tie-line and ACE must be incorporated into the control area structure in order to simulate the deregulated environment. The complete block diagram for a control area in a deregulated environment is shown in Figure 3. It is shown from Figure 3 that the new tie-line power has incorporated the demand of different discos in the same and other areas to form ACE. Further, the control scheme has to take care of different transactions within the area as well as outside the area to regulate the Gencos generation.
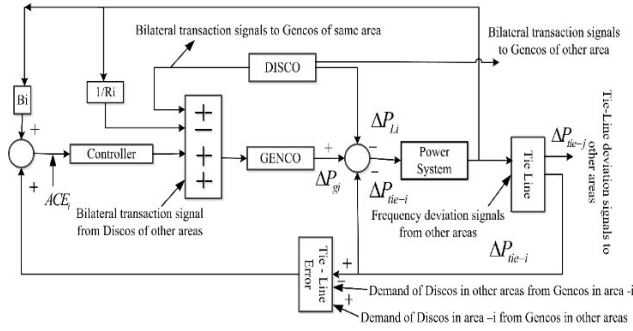
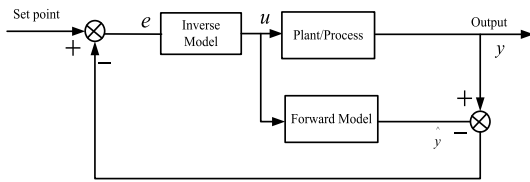**FIGURE 3.** Block diagram of LFC scheme of an area under deregulated environment.

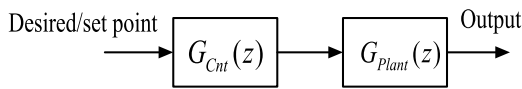**FIGURE 4.** NN based IMC structure.

FIGURE 5. Open loop control strategy.

III. CONTROL SCHEMES

In this paper, two control schemes, namely NN-IMC and fractional order PID (FO-PID) have been designed. The performance of both the designed control schemes has been checked on a 75-bus, 15-generator (four-area) power system.

A. NEURAL NETWORK-BASED INTERNAL MODEL CONTROL (NN-IMC)

The structure of IMC uses both a forward and an inverse plant model. The forward model is placed in parallel with the plant, and the difference between the plant output and the forward model output acts as the feedback signal. This signal is used by the controller, which is designed to be an inverse model of the plant. The IMC structure is shown in Figure 4. In this work, the NN approach is used to develop the forward and inverse models of the plant.

1) MODELLING OF NN - IMC

Let $\hat{G}_{Plant}(z)$ and $\hat{G}_{Plant}(z^{-1})$ represent the forward and inverse model of the plant $G_{Plant}(z)$. Figure 5 represents the open-loop control scheme of the plant known as direct inverse control (DIC) scheme, where $G_{Cnt}(z)$ is the controller used to control the plant $G_{Plant}(z)$. In the DIC scheme, the controller is to be the inverse of the plant, i.e. $G_{Cnt}(z) = \hat{G}_{Plant}(z^{-1})$. For the ideal control performance, complete knowledge of the plant is necessary.
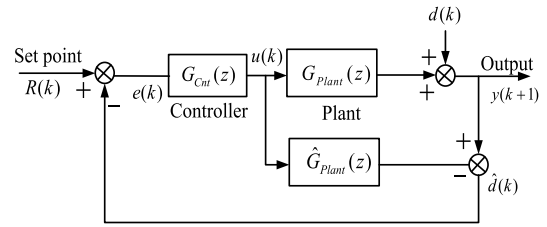

FIGURE 6. The basic structure of NN-IMC scheme.

The limitations of DIC are high sensitivity to disturbances and noise and the inability to control the unstable system. The problems with the DIC approach can be eliminated using the IMC approach. IMC is an extension of the DIC scheme. The general scheme of IMC is shown in Figure 6.

Where $d(k)$ = unknown disturbance and $u(k)$ = input to both the plant/model.

The plant output $y(k + 1)$ is compared with the output of the forward model, resulting in a signal $\hat{d}(k)$.

$$\hat{d}(k) = [G_{Plant}(z) - \hat{G}_{Plant}(z)]u(k) + d(k) \qquad (5)$$

If $d(k)$ is zero, then $\hat{d}(k)$ is a measure of the difference in behavior between the plant and its forward model. Thus, $\hat{d}(k)$ can be the missing information in the model $\hat{G}_{Plant}(z)$ and can therefore be used to improve control. This is done by subtracting $\hat{d}(k)$ from the setpoint $R(k)$. The resulting control signal is given as,

$$u(k) = [R(k) - \hat{d}(k)]G_{Cnt}(z)$$
$$= \left\{ R(k) - \left[G_{Plant}(z) - \hat{G}_{Plant}(z) \right] u(k) - d(k) \right\} G_{Cnt}(z) \qquad (6)$$

Thus,

$$u(k) = \frac{\lceil R(k) - d(k) \rceil G_{Cnt}(z)}{1 + \left[G_{Plant}(z) - \hat{G}_{Plant}(z) \right] G_{Cnt}(z)} \qquad (7)$$

Since,

$$Y(k) = G_{Plant}(z)u(k) + d(k) \qquad (8)$$

The output of the IMC scheme is

$$Y(k) = \frac{[R(k) - d(k)] G_{Cnt}(z)G_{Plant}(z)}{1 + \left[G_{Plant}(z) - \hat{G}_{Plant}(z) \right] G_{Cnt}(z)} + d(k) \qquad (9)$$

Or

$$Y(k) = \frac{G_{Cnt}(z)G_{Plant}(z)R(k) + \left[1 - G_{Cnt}(z)\hat{G}_{Plant}(z) \right] d(k)}{1 + \left[G_{Plant}(z) - \hat{G}_{Plant}(z) \right] G_{Cnt}(z)} \qquad (10)$$

From the close loop expression, it is evident that if $G_{Cnt}(z) = \hat{G}_{Plant}(z^{-1})$, and $G_{Plant}(z) = \hat{G}_{Plant}(z)$, then the perfect desired point tracking can be achieved. The perfect implementation of the NN-IMC approach relies on the accuracy of the forward and inverse models. The implementation of NN-IMC is shown in Figure 7.
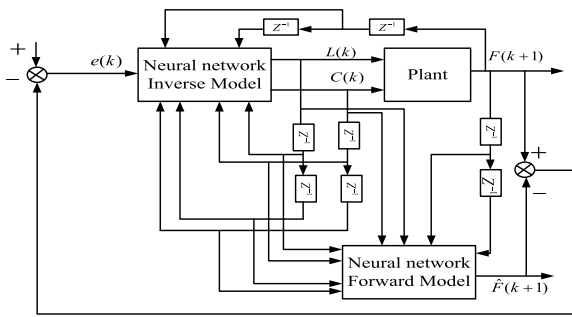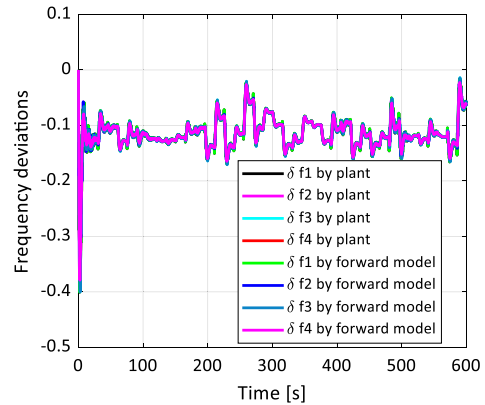
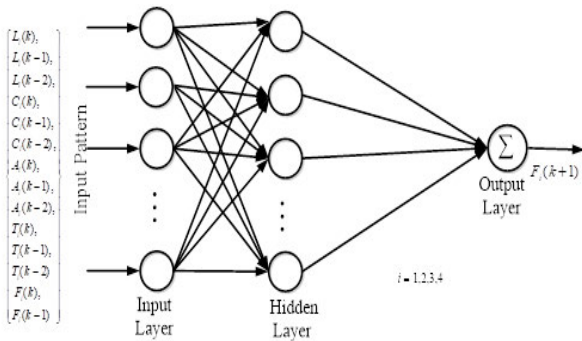**FIGURE 7.** The structure of NN-IMC scheme.

FIGURE 8. Forward model of four-area AGC scheme.

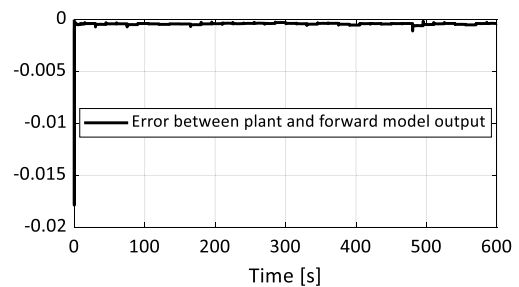**FIGURE 9.** Plant output and forward model output.

FIGURE 10. Error between plant and forward model output.

2) DESIGNING OF FORWARD AND INVERSE MODELS OF TEST SYSTEM

To design a forward model, inputs and outputs of a four-area power system have been. The inputs of the forward model are the present and time-delayed values of load perturbations, area control errors, reference power setting, tie-line power and frequency deviations from area-1 to area-4. The predicted values of frequencies in area-1 to area-4 are the output of the forward model. The architecture used for the training of the forward model is shown in Figure 8.

Where, $L(k)$ represents load perturbation, $C(k)$ is change in reference power, $A(k)$ is the area control error, $T(k)$ is the tie-line power deviation and $F(k)$ is the frequency deviation. The L-M algorithm is used for training. The number of neurons in the input layer is 56. The number of hidden nodes is 20. The sigmoidal and linear activation functions for the hidden and output layers have been chosen. The learning rate and the number of training epochs are selected as 0.01 and 500, respectively. The predicted output of the forward model is compared with the plant output in Figure 9. The error between the predicted output and the actual output is shown in Figure 10.

The inputs of the inverse model are the error e(k), the past values of load perturbations, reference power setting, frequency deviations, area control error and tie-line power deviations in area-1 to area-4. The output of the inverse model is the present values of the reference power setting from area-1 to area-4. The training of the inverse model has been done
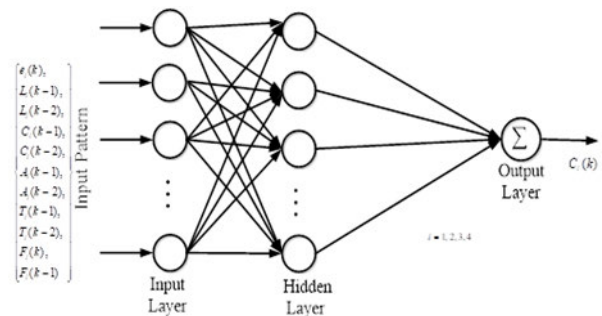

FIGURE 11. Inverse model of four-area AGC scheme.

in the same way as for the forward model. The number of neurons in the input layer is 41. The number of hidden nodes is 20. The learning rate is 0.01 and the number of epochs is 500. The L-M algorithm is used for training the model. The architecture of the inverse model network is shown in Figure 11.

B. FO-PID CONTROL SCHEME USING BBBC

The basis of the thought of FO-PID is the PID controller. FO-PID is an extension of PID where one can design a better control scheme in order to reduce steady-state error, oscillation and settling time. The most common structure of an FO-PID is shown in Figure 12 [25].
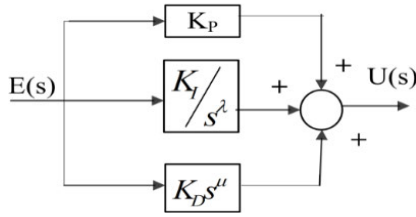
FIGURE 12. FO-PID structure.

Where,

$$u(t) = K_P e_r(t) + K_I D^{-\lambda} e_r(t) + K_D D^\mu e_r(t) \quad (11)$$

The Laplace form of the FO-PID controller can be represented as,

$$G_{\text{FO-PID}}(s) = K_P + K_I s^{-\lambda} + K_D s^\mu \quad (12)$$

where, K_P, K_I, and K_D = FO-PID parameters, λ/μ are fractional integrator/differentiator.

For effective performance of FO-PID, its parameters should be obtained optimally. Therefore, in this work, the BBBC algorithm is used to determine parameters by minimizing the fitness function, given in (13).

$$F = \frac{1}{n} \sum_{i=1}^{n} [(ACE_i)^2] \quad (13)$$

- Steps to design FO-PID using BBBC [24]–[27]

Step 1. This step involves the generation of the population of parameters as per (14).

$$x_{ij}^{(k)} = x_{i(\min)}^{(k)} + \text{rand.}(x_{i(\max)}^{(k)} - x_{i(\min)}^{(k)}) \quad (14)$$

where, x = FO-PID parameters, k = total number of areas, i = total parameters, j = total population size

Step 2. In this step, fitness function (13) is evaluated for the population generated in step 1.

Step 3. This steps involves in creation of the center of mass given (15).

$$X_{\text{com}} = \frac{\sum_{j=1}^{p} \frac{x_{ij}^{(k)}}{F_j}}{\sum_{j=1}^{p} \frac{1}{F_j}} \quad (15)$$

Step 4. In this step, a new population is created in the vicinity of the center of mass determined in the earlier step

$$x_{ij(\text{new})}^{k} = X_{\text{com}} + \frac{r.\alpha(x_{i(\max)}^{k} - x_{i(\min)}^{k})}{K} \quad (16)$$

where, α = Parameter limit the size, r = Random number, K = Iteration number.

Step 5. This step involves the generation of the next best parameters

$$x_{ij(\text{next})}^{k} = \min \left\{ F(x_{ij(\text{previous})}^{k}), F(x_{ij(\text{new})}^{k}) \right\} \quad (17)$$
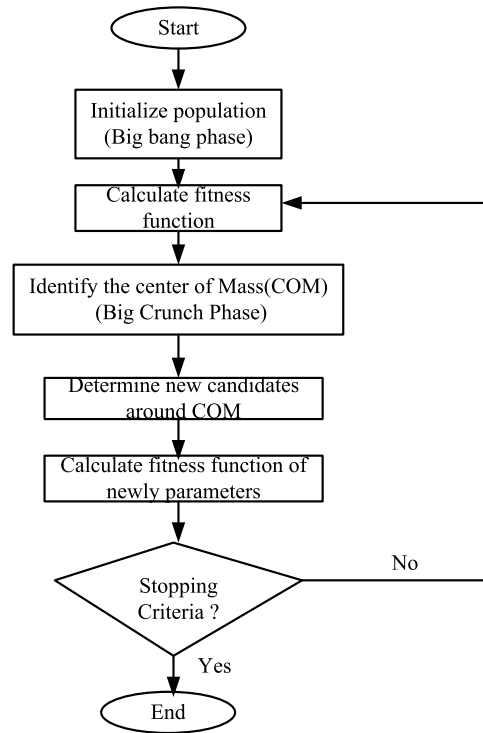

FIGURE 13. General flowchart of BBBC algorithm.

Step 6. This step determines the best fitness function and its associated parameters.

The genral flowchart of BBBC algorithm is shown in Figure 13.

IV. SIMULATION RESULTS

The performance of both the designed control schemes has been evaluated on a 75-bus, 15-generator hydrothermal power system [26]. The modelling of the test system has been done as per section 2. This test system consists of four control areas. Area–1 has 3 Gencos and a total rating of 460MW. Area–2 has 5 Gencos and is rated at 994MW. Area–3 has a capacity of 400MW and 2 Gencos, whereas Area–4 has a capacity of 4470MW and 5 Gencos. In each area, 3 discos have been considered. In order to investigate various cases, Poolco and bilateral transactions have been considered.

A. CASE 1: MIXED TRANSACTION

Mixed transactions are simulated by assuming that all Gencos and Discos are participating in the market. The bids (price and capacity) submitted by Gencos and Discos are given in [26], [27]. In this case, a step rise load of 50MW (0.1087pu) in area-1, 50MW (0.0503pu) in area-2, 0.125pu (50MW) in area-3 and 0.0224pu (100MW) in area-4 has been assumed at time t = 0. To meet this demand following bilateral transactions have been considered.

1. Area-2's Genco5 (G5) has a contract to deliver 10% of area-1's load requirement.

TABLE 1. Participation factors(PF) of gencos (G).

Area	Area-1	Area-2	Area-3	Area-4
G	G1/G2	G6/G8	G9/G10	G11/G13/G15
pf	.6667/.1111	.1429/.7143	.3/.7	.3571/.1429/.3571

TABLE 2. Participation factors of discos.

Area	Area-1	Area-2	Area-4
Discos(D)	D1	D6	D11
pf	0.2222	0.1429	0.1429

2. Area-4's Genco11(G11) has a contract to deliver 20% of area-2's load requirement.
3. Area-2's Genco4 (G4) has a contract to supply 10% of the demand.
4. Area-2's Genco5 (G5) has been contracted to deliver 10% of area-4's load.
5. Area-4's Genco12 (G12) has a contract to supply 20% of the area's load requirement.

After following bilateral contracts, the powers demanded in the each area are as: Area-1/45MW, Area-2/35MW, Area-3/0MW, Area-4/70MW. To satisfy this additional demand, the Poolco contract has been simulated. To implement the Poolco transactions, the participation factors of Gencos and Discos are calculated and given in Table 1 and Table 2 respectively.

After implementing the above transactions, participation factors, load demands, and the following results have been obtained using MATLAB simulation. Frequency deviation in different areas is shown in Figure 14. It is seen that on a load perturbation, the frequency of each area deviates from its scheduled value. However, by that time, it settles to its desired value at a steadystate. It is also evident from Figure 13 that the frequency of each area has a shorter settling time with the NN-IMC control scheme than with the FO-PID control scheme.

The net change in Gencos and Discos of each area can be calculated in the following manner:

In area-1: Gencos (G1 G2 and G3) do not engage in bilateral transactions and change their generation as per Poolco transactions. As per bilateral transaction, 10% i.e. 5MW of the total load (50 MW) of area-1 is supplied by G5 of area-2. Therefore, the remaining load (45MW) of area-1 is supplied by G1, G2, and D1 as per their Poolco participation. In order to fulfill the remaining requirements of area-1, G1 and G2 regulate their generation by 30MW (0.6667*45) and 5MW (0.111*45). Therefore, a total of 35 MW out of 45 MW is provided by Gencos G1-G2. To provide the remaining 10 MW, Disco D1 reduces its load by 10MW (0.2222*45). The change in the Gencos and Discos of area-1 is shown in Figure 15.

In area-2: Gencos (G4, G5) have bilateral whereas Gencos (G6, G8) have Poolco transactions. To meet the bilateral
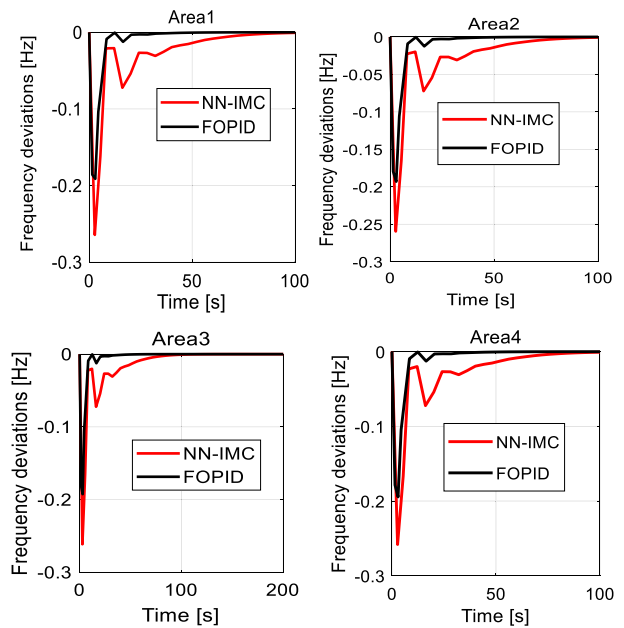
FIGURE 14. Frequency deviations in areas (1-4) (Hz).
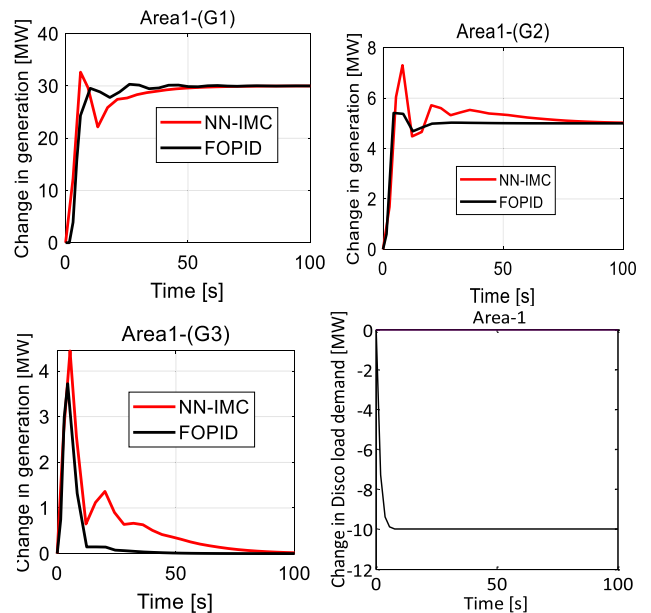
FIGURE 15. Change in gencos-discos of area-1 (MW).

contract of 10% (5MW) of total load (50MW) of area-2, G4 regulates its generation by 5MW. G5 regulates its generation by 15MW in order to provide 10% (5MW) of area-1 total load (50MW) and 10% (10MW) of area-4 total load (100MW). The remaining load of 35MW of area-2 is supplied by G6, G8, and Disco D6 as per their participation. G6 regulates its generation by 5MW (0.1429*35), G8 by 25MW (0.7143*35) and Disco D6 reduces its demand by 5MW (0.1429*35).

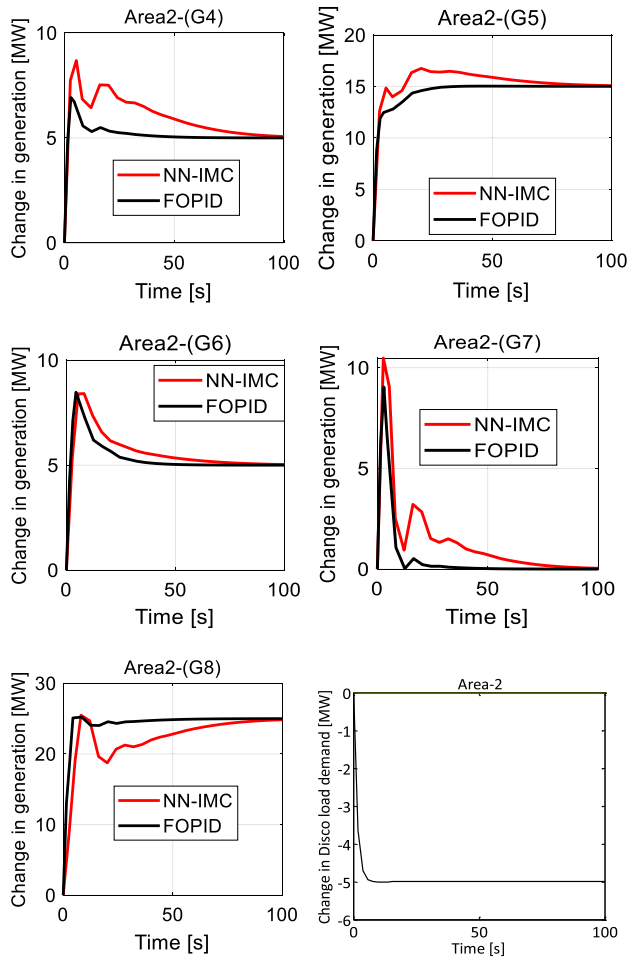**In area-3:** Gencos G9 and G10 only have a Poolco contract to satisfy the demand of 50MW of area-3. Therefore, G9

FIGURE 16. Change in gencos-disco of area-2 (MW).

FIGURE 17. Change in gencos of area-3 (MW).

FIGURE 18. Change in gencos-discos of area-4 (MW).

regulates its generation by 15MW (0.3*50) and G10 increases its generation by 35MW (0.7*50).

In area-4: The Genco G11 of area-4 provides 20% (10MW) of area-2 load (50MW) using bilateral transactions. A total of 30% (30MW) of the load (100MW) of area-4 is provided by the Gencos (G12-20%, G5-10%) using bilateral transactions. Therefore, G12 changes its generation by 20MW and G5 changes its generation by 10MW. The rest of the load (70MW) of area-4 is shared by G11, G13, G15, and D11 of area-4, as per their Poolco factors. To satisfy this demand, G11 changes to 25MW (0.3571*70), G13-10MW (0.1429*70), G15-25MW (0.3571*70) and D1-10MW (0.1429*70).

The change in Gencos from area-2 to area-4 is shown in Figure 16 to Figure 18, respectively. The tie-line power deviations are not settled to zero because of bilateral transactions. Figure 18 shows the tie-line deviations in the respective areas.

The performance of NN-IMC and FO-PID control schemes has also been checked in terms of maximum overshoot/undershoot and settling time of frequency deviation of area-1 and area-4 and is given in Table 3.
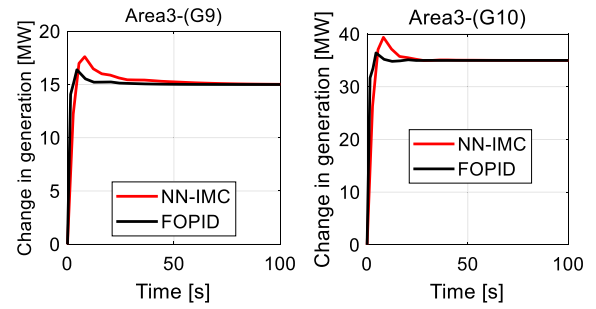
B. CASE 2: CONTRACT VIOLATION

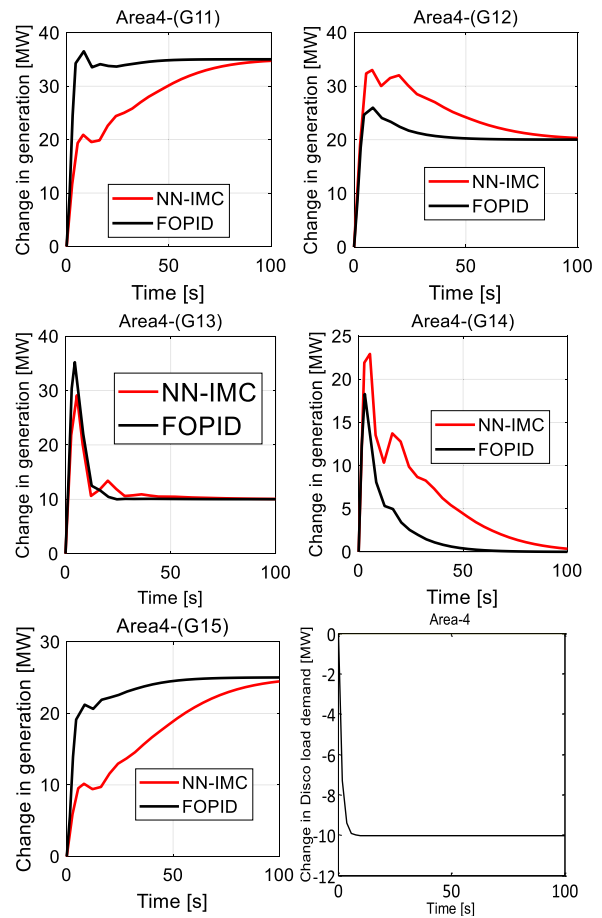In this case, it is considered that G5 of area-2 violates the contract with Discos of area-1 and area-4. Instead of supplying 10% of demand of area-1 (5MW) and 10% demand of area-4 (10MW), it supplies only 5% of the load demand of area-1 and 5% of the demand of area-4. Due to this contract violation, area-1 and area-4 have a power deficit of 2.5MW and 5MW, respectively. In the previous case, 45MW of area-1 power was met by the Poolco transaction, while in this case, 47.5MW will be provided by the Poolco transactions. Similarly, instead of 70MW of power in area-4, 75MW of

TABLE 3. Performance parameters for frequency deviations.

	Controller	Max. undershoot (area-1)	Max. overshoot (area-1)	Settling time (sec.)
	NN-IMC	-0.252	0.0	90
Mixed	FO-PID	-0.19	0.0	60
Transaction	Controller	Max. Undershoot (Area-4)	Max. Overshoot (Area-4)	Settling Time (Sec.)
	NN-IMC	-0.252	0.0	95
	FO-PID	-0.195	0.0	65

FIGURE 19. Tie-line power deviations in areas (1-4) (MW).

FIGURE 20. Frequency deviations in areas (1-4) (Hz).
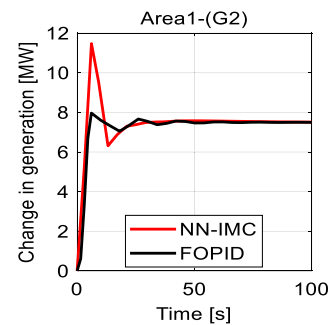
FIGURE 21. Change in G2 in area-1(MW).
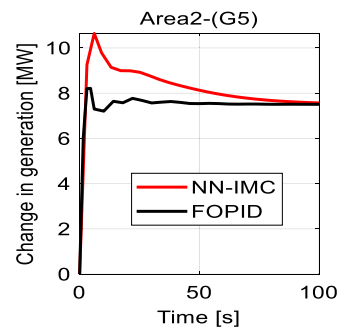
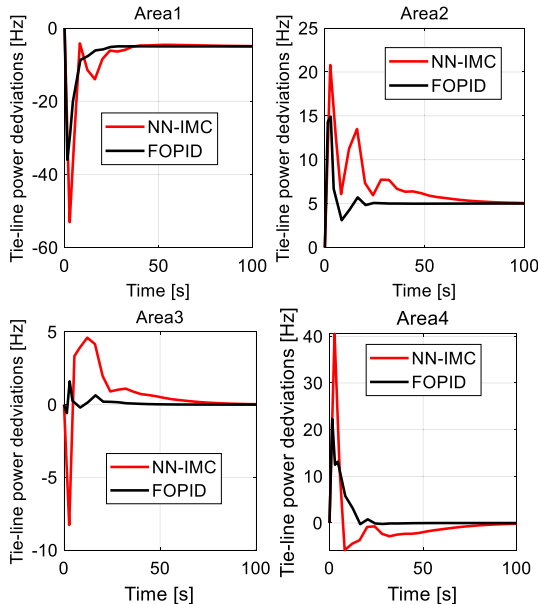**FIGURE 22.** Change in G5 in area-2 (MW).

power will be provided by Poolco transactions. This power will be arranged by the system operator through Poolco transactions. Frequency deviations with NN-IMC and FO-PID control schemes from area-1 to area-4 are shown in Figure 20. It is seen that frequency deviations in all the areas finally settle to zero.

Due to the contract violation of G5, the following changes will occur in the real power generation of different Gencos in comparison to the previous case.

In area-1: The change in generation of G1 remains at 30MW, the same as in the previous case. The change in generation of G2 has been increased by 2.5MW, i.e., net 7.5MW due to contract violation as shown in Figure 21. **In area-2:** The changes in the generation of Gencos (G4, G6, G7, and G8) of area-2 remain the same as in the previous case. Only Genco G5 in area-2 changes output by 7.5MW to fulfill 5% of area-1 load (50MW) and 5% of area-4 load (100MW), as shown in Figure 22. **In area-3:** The change in the generation of Gencos in area-3 remains same as in the previous case. **In area-4:** The excess demand of 5MW will be supplied by G13, which changes its generation from 10MW to 15MW. The change in the real power output of G13 in area-4 is shown in Figure 23. The remaining Gencos (G11, G12, G14, G15) and D11 in area-4 change their generation and load, the same as in the previous case. Figure 24 shows
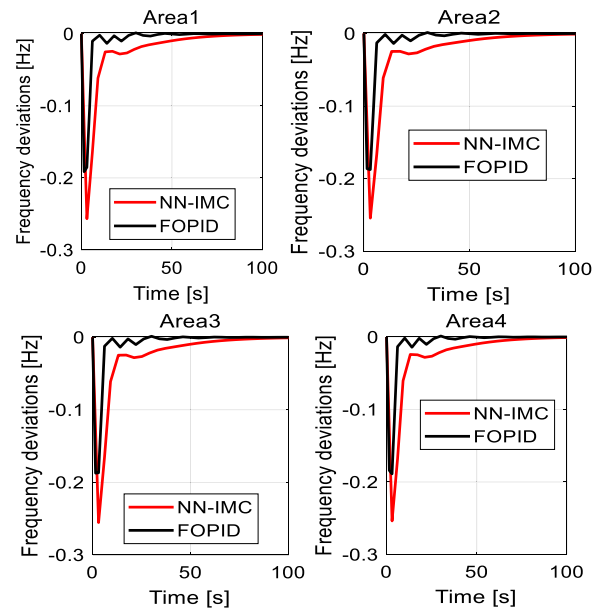
the tie-line power deviations among all areas. Table 4 compares the performance of both control schemes for contract violation cases.

V. NERC STANDARDS COMPLIANCE
In this section, the compliance of the NN-IMC controller with NERC control standards has been checked [29]. Relative compliance has been established on 75-bus four-area power system. The considered load variation is given in Figure 25. An average frequency deviation at 10-minute time intervals for both the controllers is shown in Figure 26. The com-

FIGURE 23. Change in G13 in area-4 (MW).
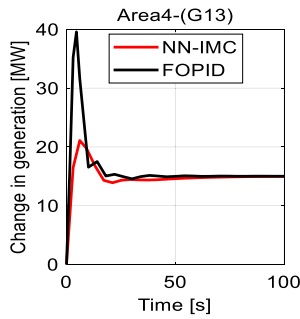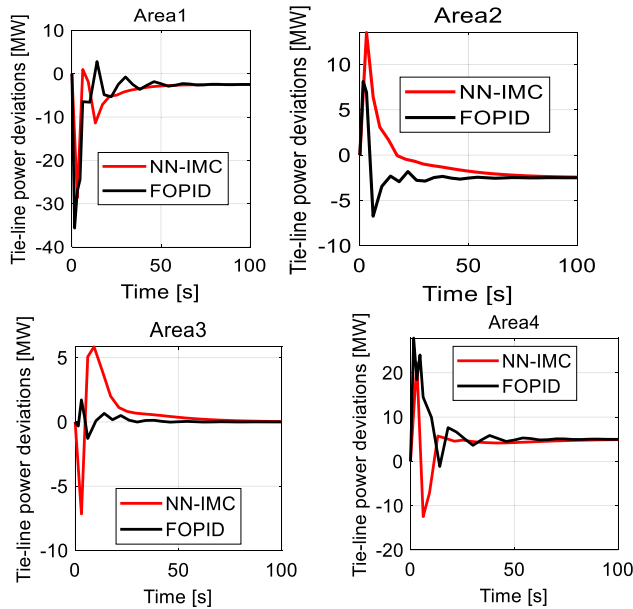

FIGURE 24. Tie-line power deviations in areas (1-4) (MW).

TABLE 4. Performance parameters for frequency deviations.

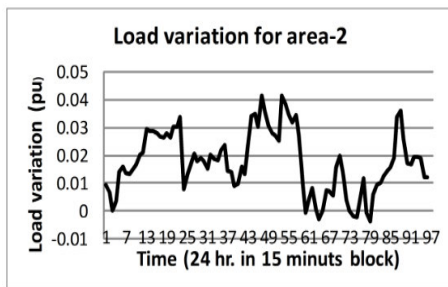|	Controller	Max. undershoot (area-1)	Max. overshoot (area-1)	Settling time (sec.)
	NN-IMC	-0.251	0.0	90
Contract	FO-PID	-0.1915	0.0014	65
Violation	Controller	Max. undershoot (area-4)	Max. overshoot (area-4)	Settling time (sec.)
	NN-IMC	-0.251	0.0	95
	FO-PID	-0.1888	0.00135	75

FIGURE 25. Load variation for area-2.

parative values of CF calculated for both the controllers are shown in Figure 27. Using these values of CF, CPS1 values have been determined for NN-IMC and FO-PID controllers as given in Figure 28, which shows that CPS1 is satisfied
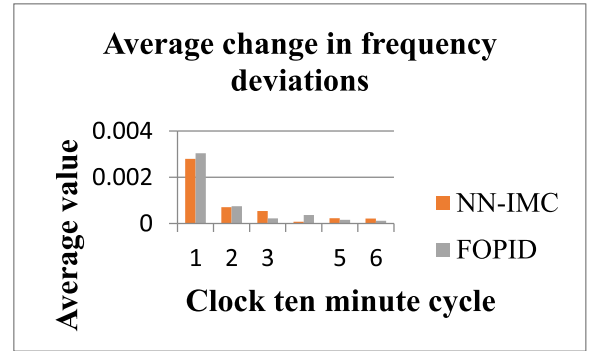

FIGURE 26. Average change in frequency deviations at 10-minute time interval.
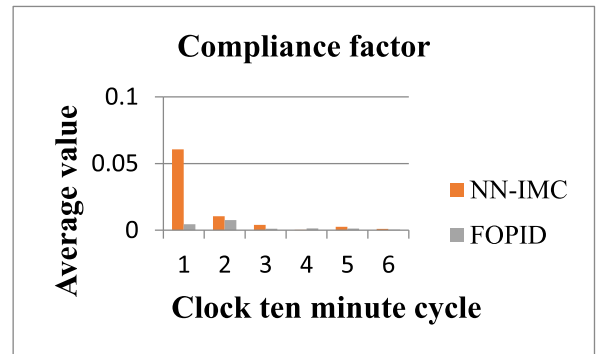
FIGURE 27. Computed values of CF.
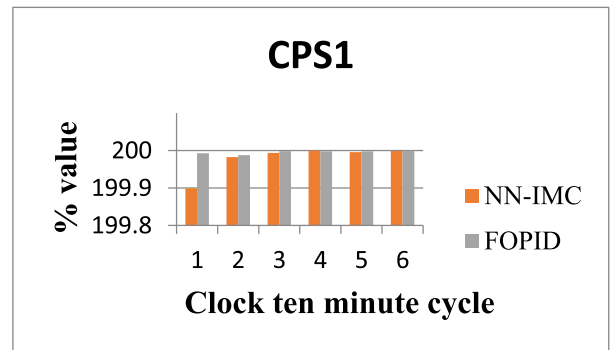
FIGURE 28. Comparative values of CPS1.

for both the controllers but the relative compliance is better in case of the FO-PID controller. The values of the ACE average are shown in Figure 29. On comparing these values with limit L_{10}, it is seen that no violation has been recorded by the NN-IMC and FO-PID controllers. Therefore, CPS2 is satisfied for both the controllers, as given in Figure 30.

VI. CONCLUSION
A general-purpose NN-IMC scheme suitable for deregulated power systems has been proposed in this paper. The NN-IMC scheme has been implemented to meet the Poolco and bilateral transactions. This scheme has been successfully tested on a 75-bus, 15 generators (four-area) power system. Two cases, i.e. normal and contract violation, have been simulated to investigate the performance of the designed control scheme. It is seen that the frequency errors are eliminated at a steady-state, as well as Gencos and Discos share the demand as per

FIGURE 29. Violation of L10 limit.

FIGURE 30. Comparative values of CPS2.

their mixed contracts. The results show that the NN-IMC control scheme has good performance and improves system responses effectively. Further, the NN-IMC control scheme results have also been compared with the results of the FO-PID con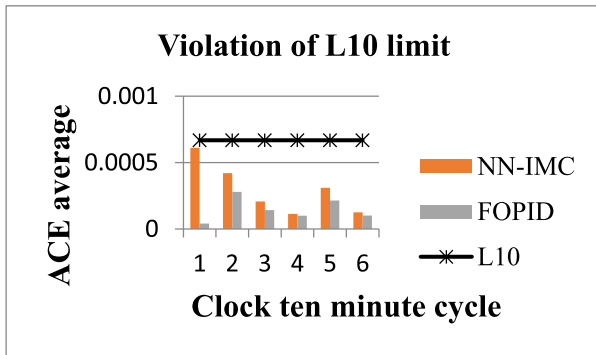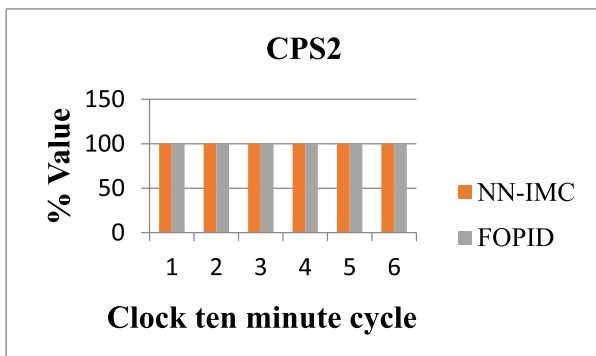trol scheme. It is observed that the performance of both the control schemes is satisfactory. However, NN-IMC outperforms FO-PID in terms of settling time and maximum overshoots/undershoots. The compliance of the NN-IMC scheme has also been checked with NERC standards. It is seen that the NN-IMC scheme also satisfied the CPS1 and CPS2 control standards. Therefore, NN-IMC can be suited as an LFC scheme for multi area power systems in a deregulated environment.

REFERENCES

[1] O. Elgerd and C. Fosha, "Optimum megawatt-frequency control of multi-area electric energy systems," *IEEE Trans. Power App. Syst.*, vol. PAS-89, no. 4, pp. 556–563, Apr. 1970, doi: 10.1109/TPAS.1970.292602.

[2] R. D. Christie and A. Bose, "Load frequency control issues in power system operations after deregulation," *IEEE Trans. Power Syst.*, vol. 11, no. 3, pp. 1191–1200, Aug. 1996, doi: 10.1109/59.535590.

[3] H. H. Alhelou, M.-E. Hamedani-Golshan, R. Zamani, E. Heydarian-Forushani, and P. Siano, "Challenges and opportunities of load frequency control in conventional, modern and future smart power systems: A comprehensive review," *Energies*, vol. 11, no. 10, pp. 1–35, 2018, doi: 10.3390/en11102497.

[4] G. S. da Silva, E. J. de Oliveira, L. W. de Oliveira, A. N. de Paula, J. S. Ferreira, and L. M. Honório, "Load frequency control and tie-line damping via virtual synchronous generator," *Int. J. Electr. Power Energy Syst.*, vol. 32, pp. 1–14, Nov. 2021, doi: 10.1016/j.ijepes.2021.107108.

[5] T. H. Mohamed, M. A. M. Alamin, and A. M. Hassan, "A novel adaptive load frequency control in single and interconnected power systems," *Ain Shams Eng. J.*, vol. 12, no. 2, pp. 1763–1773, Jun. 2021, doi: 10.1016/j.asej.2020.08.024.

[6] W. Tan, "Tuning of PID load frequency controller for power systems," *Energ. Convers. Manage.*, vol. 50, pp. 1465–1472, Jun. 2009, doi: 10.1016/j.enconman.2009.02.024.

[7] M. Bhuyan, A. K. Barik, and D. C. Das, "GOA optimised frequency control of solar-thermal/sea-wave/biodiesel generator based interconnected hybrid microgrids with DC link," *Int. J. Sustain. Energy*, vol. 39, no. 7, pp. 1–19, 2020, doi: 10.1080/14786451.2020.1741589.

[8] S. Nag and N. Philip, "Application of neural networks to automatic load frequency control," in *Proc. Int. Conf. Control, Instrum., Energy Commun. (CIEC)*, Jan. 2014, pp. 345–350.

[9] B. Ogbonna and S. N. Ndubisi, "Neural network based load frequency control for restructuring power industry," *Nigerian J. Technol.*, vol. 31, no. 1, pp. 40–47, 2012.

[10] S. Saxena and Y. V. Hote, "Internal model control based PID tuning using first-order filter," *Int. J. Control, Autom. Syst.*, vol. 15, no. 1, pp. 149–159, Feb. 2017, doi: 10.1007/s12555-015-0115-y.

[11] W. Tan, "Unified tuning of PID load frequency controller for power systems via IMC," *IEEE Trans. Power Syst.*, vol. 25, no. 1, pp. 341–350, Feb. 2010, doi: 10.1109/TPWRS.2009.203646.

[12] S. Saxena and Y. V. Hote, "Load frequency control in power systems via internal model control scheme and model-order reduction," *IEEE Trans. Power Syst.*, vol. 28, no. 3, pp. 2749–2757, Aug. 2013, doi: 10.1109/TPWRS.2013.2245349.

[13] R. Lamba, S. Sondhi, and K. S. Singla, "Reduced order model based FOPID controller design for power control in pressurized heavy water reactor with specific gain–phase margin," *Prog. Nucl. Energy*, vol. 125, pp. 1–19, Jul. 2020, doi: 10.1016/j.pnucene.2020.103363.

[14] S. E. Hamamci, "An algorithm for stabilization of fractional-order time delay systems using fractional-order PID controllers," *IEEE Trans. Autom. Control*, vol. 52, no. 10, pp. 1964–1969, Oct. 2017, doi: 10.1109/TAC.2007.906243.

[15] F. Yang, X. Shao, S. M. Muyeen, D. Li, S. Lin, and C. Fang, "Disturbance observer based fractional-order integral sliding mode frequency control strategy for interconnected power system," *IEEE Trans. Power Syst.*, vol. 36, no. 6, pp. 5922–5932, Nov. 2021, doi: 10.1109/TPWRS.2021.3081737.

[16] S. Oshnoei, A. Oshnoei, A. Mosallanejad, and F. Haghjoo, "Contribution of GCSC to regulate the frequency in multi-area power systems considering time delays: A new control outline based on fractional order controllers," *Int. J. Electr. Power Energy Syst.*, vol. 123, Dec. 2020, Art. no. 106197.

[17] Z. Yan and Y. Xu, "A multi-agent deep reinforcement learning method for cooperative load frequency control of a multi-area power system," *IEEE Trans. Power Syst.*, vol. 35, no. 6, pp. 4599–4608, Nov. 2020.

[18] A. Oshnoei, M. Kheradmandi, and S. M. Muyeen, "Robust control scheme for distributed battery energy storage systems in load frequency control," *IEEE Trans. Power Syst.*, vol. 35, no. 6, pp. 4781–4791, Nov. 2020.

[19] A. Oshnoei, M. Kheradmandi, S. M. Muyeen, and N. D. Hatziargyriou, "Disturbance observer and tube-based model predictive controlled electric vehicles for frequency regulation of an isolated power grid," *IEEE Trans. Smart Grid*, vol. 12, no. 5, pp. 4351–4362, Sep. 2021.

[20] M. S. Ayas and E. Sahin, "FOPID controller with fractional filter for an automatic voltage regulator," *Comput. Electr. Eng.*, vol. 90, Mar. 2021, Art. no. 106895, doi: 10.1016/j.compeleceng.2020.106895.

[21] N. Hamouda, B. Babes, C. Hamouda, S. Kahla, T. Ellinger, and J. Petzoldt, "Optimal tuning of fractional order proportional integral derivative controller for wire feeder system using ant colony optimization," *J. Eur. Syst. Automn.*, vol. 53, no. 2, pp. 157–166, 2020, doi: 10.18280/jesa.530201.

[22] S. Debbarma, L. C. Saikia, and N. Sinha, "AGC of a multi-area thermal system under deregulated environment using a non-integer controller," *Electr. Power Syst. Res.*, vol. 95, pp. 175–183, Feb. 2013, doi: 10.1016/j.epsr.2012.09.008.

[23] E. Yesil, "Interval type-2 fuzzy PID load frequency controller using big bang-big crunch optimization," *Appl. Soft Comput.*, vol. 15, pp. 100–112, Feb. 2014, doi: 10.1016/j.asoc.2013.10.031.

[24] N. Kumar, B. Tyagi, and V. Kumar, "Multiarea deregulated automatic generation control scheme of power system using imperialist competitive algorithm based robust controller," *IETE J. Res.*, vol. 64, no. 4, pp. 528–537, Jul. 2018, doi: 10.1080/03772063.2017.1362965.

[25] N. Kumar, V. Kumar, and B. Tyagi, "Multi area AGC scheme using imperialist competition algorithm in restructured power system," *Appl. Soft Comput.*, vol. 48, pp. 160–168, Nov. 2016, doi: 10.1016/j.asoc.2016.07.005.

[26] N. Kumar, B. Tyagi, and V. Kumar, "Deregulated multiarea AGC scheme using BBBC-FOPID controller," *Arabian J. Sci. Eng.*, vol. 42, no. 7, pp. 2641–2649, Jul. 2017, doi: 10.1007/S13369-016-2293-1.

[27] N. Kumar, B. Tyagi, and V. Kumar, "Deregulated multiarea AGC scheme using BBBC-FOPID controller," *Arabian J. Sci. Eng.*, vol. 42, no. 7, pp. 2641–2649, Jul. 2017, doi: 10.1007/s13369-016-2293-1.

[28] V. Donde, M. A. Pai, and I. A. Hiskens, "Simulation and optimization in an AGC system after deregulation," *IEEE Trans. Power Syst.*, vol. 16, no. 3, pp. 481–489, Aug. 2001, doi: 10.1109/59.932285.

[29] T. Sasaki and K. Enomoto, "Dynamic analysis of generation control performance standards," *IEEE Trans. Power Syst.*, vol. 17, no. 3, pp. 806–811, Aug. 2002, doi: 10.1109/TPWRS.2002.80094.

NAGENDRA KUMAR received the M.Tech. degree from the National Institute of Technology (NIT) Hamirpur, India, in 2010, and the Ph.D. degree in the area of power system from the Department of Electrical Engineering, Institute of Technology (IIT) Roorkee, India, in 2017.

He is currently associated with the Electrical and Electronics Engineering Department, G. L. Bajaj Institute of Technology & Management, Greater Noida, as an Associate Professor. He is also a faculty in-charge of the Simulation based Power System Laboratory, Electrical and Electronics Engineering Department, Institute Innovative Cell, and Research & Development (R&D) Coordinator. He is also engaged in expert committee of Ph.D. research scholars of different institutions/universities. He has published several research papers in leading international journals. His research papers were presented and published as conference proceedings at several prestigious academic conferences, such as IEEE and Elsevier. His research interests include power system stability, power system deregulation, demand side management, hybrid power systems, and renewable energy.

HASMAT MALIK (Senior Member, IEEE) received the M.Tech. degree in electrical engineering from the National Institute of Technology (NIT) Hamirpur, Himachal Pradesh, India, and the Ph.D. degree in electrical engineering from the Indian Institute of Technology (IIT), Delhi.

He has worked as an Assistant Professor for more than five years with the Division of Instrumentation and Control Engineering, Netaji Subhas Institute of Technology (NSIT), Dwarka, Delhi, India. He is currently a Chartered Engineer (C.Eng.) and a Professional Engineer (P.Eng.). He is also a Research Fellow with Berkeley Education Alliance for Research in Singapore (BEARS). He has been with the Research Center, University of California at Berkeley, Berkeley, University Town, the National University of Singapore (NUS), Singapore, since January 2019. He has published widely in international journals and conferences his research findings related to intelligent data analytics, artificial intelligence, and machine learning applications in power systems, power apparatus, smart building & automation, smart grid, forecasting, prediction, and renewable energy sources. He has authored/coauthored more than 100 research papers and nine books and 13 chapters in nine other books, published by IEEE, Springer, and Elsevier. He has supervised 23 PG students. His research interests include application of artificial intelligence, machine learning and big-data analytics for renewable energy, smart building & automation, condition monitoring, and online fault detection & diagnosis (FDD).

Dr. Malik is also a member of the Institution of Engineering and Technology (IET), U.K., the Computer Science Teachers Association (CSTA), the Association for Computing Machinery (ACM) EIG, and Mir Labs, Asia, a Life Member of the Indian Society for Technical Education (ISTE), the Institution of Engineers (IEI), India, and the International Society for Research and Development (ISRD), London, and a fellow of the Institution of Electronics and Telecommunication Engineering (IETE). He received the POSOCO Power System Award (PPSA-2017) for his Ph.D. work for research and innovation in the area of power systems. He also received the Best Research Papers Awards from IEEE INDICON-2015, and the Full Registration Fee Award from IEEE SSD-2012, Germany.

AKHILESH SINGH (Member, IEEE) received the B.Tech. degree in electrical and electronics engineering from UCER, Naini Allahabad, Uttar Pradesh, India, in 2009, the M.Tech. degree in signal processing & control from the National Institute of Technology Hamirpur, Himachal Pradesh, India, in 2011. He is currently pursuing the Ph.D. degree with Uttarakhand Technical University.

He is also working as an Assistant Professor and the Head of the Department of Electrical Engineering, Seemant Institute of Technology Pithoragarh, Uttarakhand. He also held Administrative responsibilities at the institute and District Level. He is authored/coauthored eight Science citation index international journals, five patents, 14 index international journals, two edited books, and three book chapters in Springer Nature. He organized several international and national conferences, Dehradun, Uttarakhand, India. His research interests include stability analysis and performance design of fuzzy-model and neural-network-based control systems, performance optimization and topology design of neural networks, synchronization of chaotic systems, and genetic algorithm.

MAJED A. ALOTAIBI (Member, IEEE) received the B.Sc. degree in electrical engineering from King Saud University, Riyadh, Saudi Arabia, in 2010, and the M.A.Sc. and Ph.D. degrees in electrical and computer engineering from the University of Waterloo, Waterloo, Canada, in 2014 and 2018, respectively. He is currently an Assistant Professor with the Department of Electrical Engineering, King Saud University and the Director of Saudi Electricity Company Chair for Power System Reliability and Security. He is also working as the Vice Dean of academic affairs with the College of Engineering, King Saud University. He has worked as an Electrical Design Engineer with ABB Saudi Arabia. His research interests include power system planning, operation, renewable energy modeling, applied optimization, and smart grid. He has served as a Reviewer for the IEEE Transactions on Power Systems and the IEEE Transactions on Smart Grids.

MOHAMMED E. NASSAR (Member, IEEE) was born in Alexandria, Egypt, in 1984. He received the B.Sc. and M.Sc. degrees (Hons.) in electrical engineering from Alexandria University, Alexandria, in 2006 and 2010, respectively, and the Ph.D. degree in electrical and computer engineering from the University of Waterloo, Waterloo, ON, Canada, in 2017. He is currently a definite-term Lecturer with the Department of Electrical and Computer Engineering, University of Waterloo. His research interests include electrical machines and drives, distributed and renewable generation, self-healing, smart microgrids, blockchain-based electricity markets, and smart distribution systems. He was a recipient of the AETS, EngSoc, WUSA, and OUSA teaching excellence awards.

• • •